



Effect of Thermophoresis, Brownian and Turbulent Mass Fluxes in the Simulation of Two-Phase Turbulent Free Convection of Nanofluid Inside the Enclosure using v^2 - f Model

S. Yekani Motlagh

Faculty of Mechanical Engineering, Urmia University of Technology (UUT), Urmia, Iran

ABSTRACT: In this article, two-phase alumina-water turbulent natural convection with Reynolds-averaged Navier-Stokes based v^2 - f model in a square cavity has been investigated. Buongiorno's two-phase model is modified for considering the nanoparticles diffusion via turbulent flow eddies. Using the finite volume method and the semi-implicit method for pressure-linked equations algorithm, the governing equations along with boundary conditions have been discretized. The left and right vertical walls of the cavity are kept at constant temperatures, while the other walls are thermally insulated. Calculations are performed for high Rayleigh numbers (10^7 – 10^9) and average volume fractions of nanoparticles (0 - 0.04). The results are analyzed through the thermal and dynamical fields with a particular interest in the turbulent intensity, turbulent kinetic energy, thermophoresis, Brownian and turbulent mass flux distribution inside the cavity, and Nusselt number variations. It is shown that nanoparticles had no significant effects on turbulent kinetic energy and intensity, and the thermophoresis effect is dominant at the near-wall regions. Furthermore, there are optimal average volume fractions with the maximum heat transfer rate depending on the Rayleigh number. Moreover, the magnitude of the turbulent Schmidt number had a negligible effect on the estimation of heat transfer rate. Against, low turbulent Prandtl numbers predicted higher values for the Nusselt number.

Review History:

Received: Jul. 14, 2019

Revised: Jan. 07, 2020

Accepted: Jan. 26, 2020

Available Online: Aug. 09, 2020

Keywords:

Turbulent flow

Natural convection

Nanofluid

Buongiorno model

1- Introduction

The mixture of base fluid (e.g. water, oil, ethylene glycol, or propylene glycol) and nanometer-sized particles is called nanofluid. The suspending nanoparticles, typically made of metals, oxides, carbides, or carbon nanotubes, can significantly enhance the thermal conductivity of base fluid. The dispersion of solid nanoparticles in pure fluids changes their thermal conductivity and viscosity. Consequently, as a promising new generation of coolant, nanofluid has a great potential adopted in many important applications such as fuel cell [1], micro-electronics, solar collectors [2], domestic refrigerator, and food drying. One can refer to Refs. [3–5] for the latest progress in this field. Moreover, the Turbulence regime is preferable in many industrial flows mainly because of its high degree of diffusivity of mass, momentum, and thermal energy.

In recent years, studies on nanofluid flow and heat transfer in cavities and enclosures have attracted considerable attention. The majority of studies focus on the laminar flow regime. From the numerical point of view, there are two different methods for simulation of flow and heat transfer of nanofluids, namely, single-phase and two-phase. In single-phase models, it is assumed that the fluid and particles are in thermal equilibrium and move with the same velocity [6,

7]. In fact, the effect of particles' existence is considered only on effective properties of nanofluids. However, experimental studies show that the validity of the single-phase model for nanofluids is somewhat questionable [8]. In the two-phase models, the effect of Brownian motion, thermophoresis, and other interactions between carrier fluid and nanoparticles are taken into account [9, 10]. The homogenous model is one of the single-phase models in which effective properties of nanofluid are applied in the continuity, momentum, and energy equations. Therefore, more complex and nonhomogeneous methods such as two-phase models were successfully developed and employed to consider slip velocity between the base fluid and particles [11–18]. Buongiorno [11] developed a non-homogeneous equilibrium model by considering the effect of the Brownian, diffusion, and thermophoresis. He reported seven slip mechanisms in nanofluids: inertia, Brownian, diffusion, thermophoresis, diffusiophoresis, Magnus effect, fluid drainage, and gravitational settling and concluded that in the absence of turbulence, the Brownian and thermophoresis are the most important effects. In recent years, several investigations on laminar flows have been conducted based on the transport equations derived by Buongiorno. For example, Corcione et al. [12, 13] reported laminar two-phase natural convection of nanofluids inside a differentially heated cavity using Buongiorno's model by considering the thermophoresis and

*Corresponding author's email: s.yekani@uut.ac.ir



Copyrights for this article are retained by the author(s) with publishing rights granted to Amirkabir University Press. The content of this article is subject to the terms and conditions of the Creative Commons Attribution 4.0 International (CC-BY-NC 4.0) License. For more information, please visit <https://www.creativecommons.org/licenses/by-nc/4.0/legalcode>.

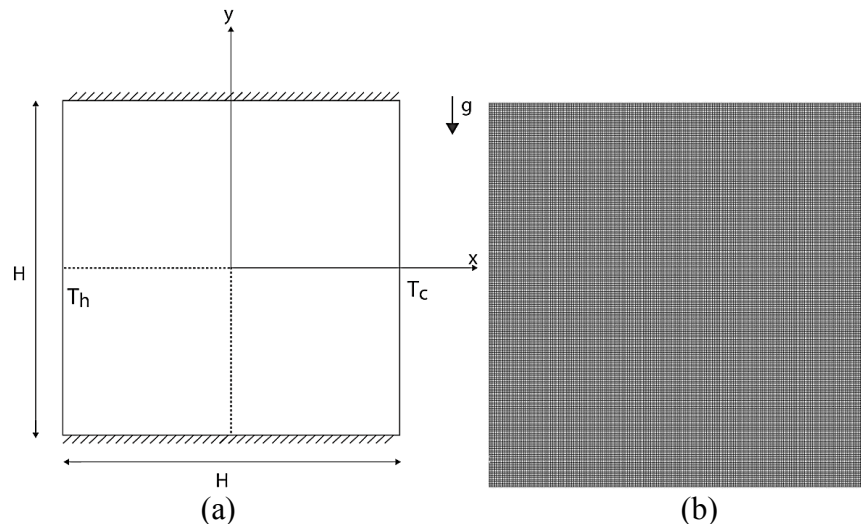


Fig. 1. (a) Geometry of cavity and (b) typical computational mesh.

Brownian diffusion of nanoparticles and concluded that the two-phase method is more accurate than the single-phase model. A similar study has been conducted by Pakravan and Yaghoubi [14], and Sheikhzadeh et al. [15] to investigate the effects of Brownian diffusion and thermophoresis in laminar free convection inside a cavity. A numerical study presented by Garoosi et al. [16] using Buongiorno's model analyzed laminar natural and mixed convection heat transfer of a nanofluid (Al_2O_3 -water) in a laterally heated square cavity. They observed that in laminar flow at low Rayleigh and high Richardson numbers, the particle distribution is fairly non-uniform while at high Rayleigh and low Richardson numbers particle distribution remains almost uniform for free and mixed convection cases, respectively. Sheremet et al. [17, 18] investigated the laminar nanofluid flow and heat transfer in porous cavities using Buongiorno's model. In their works, the effects of important parameters such as Reynolds, Grashof, Prandtl, and Lewis numbers on flow pattern and heat transfer were explored. They concluded that mentioned two mechanisms affected the nanoparticle concentration even in porous zones. Hazeri-Mahmel et al. [19] used the two-phase model for non-Newtonian fluid, successfully. Recently, Yekani Motlagh and Soltanipour [20] investigated the effect of the inclination angle of the cavity on nanoparticle distribution and heat transfer rate in laminar natural convection regimes using Buongiorno's model by considering the Brownian and thermophoresis diffusion of nanoparticles. Yekani Motlagh et al. [21,22], discussed the effect of Brownian and thermophoresis on nanoparticle distribution in the laminar two-phase free convection flow inside porous rectangular and semi annulus cavities, respectively.

The literature review showed that unlike the laminar flow of nanofluids inside cavities, very limited works have been done on turbulent nanofluid flow inside the enclosures. Besides, existing research has used a single-phase model to consider the effect of nanoparticles. Sheikhzadeh et al. [23] numerically investigated the turbulent flow inside an enclosure with a heat source and heat sink on the walls using

a single-phase model. Sajjadi et al. [24] used a single-phase model to study the heat transfer and fluid flow of nanofluids inside a tall cavity in turbulent regimes.

Based on the study above, the number of studies on turbulent free convection in the cavity is very limited, and existing studies have used single-phase models to model the effect of nanoparticles on flow. On the other hand, as mentioned earlier, the two-phase model of Buongiorno was proposed for nanoparticle penetration into the laminar flow of nanofluid, and in this model, the effect of nanoparticle diffusion due to turbulent eddies is not considered. Therefore, in the present work, Buongiorno's model was first modified and the effect of nanoparticle diffusion due to turbulent eddies was added to this model. Then, the turbulent natural convection of nanofluid flow was solved by the modified two-phase model. The effects of Rayleigh number ($10^7 \leq \text{Ra} \leq 10^9$), volume fraction ($0 \leq \phi_{\text{Ave}} \leq 0.04$), turbulent Schmidt, and Prandtl number are investigated. In this work, the Reynolds Average Navier-Stokes (RANS) based $v^2 - f$ turbulence model was used for turbulent flow analysis.

2- Mathematical Modeling

2.1 Problem statement

The schematic of the considered problem in the present investigation is shown in Fig. 1. A two-dimensional square cavity with a height of H is filled with Al_2O_3 -water nanofluid. The top and bottom walls are thermally insulated whereas the two vertical walls are at constant but different temperatures T_h and T_c , respectively. As shown, the gravity force acts in the vertical direction.

2.2 Dimensional governing equations and boundary conditions

The flow is assumed two dimensional, incompressible, and stationary turbulent. Nanoparticles are considered to have uniform shape and size and in thermal equilibrium with the base fluid. The density variation with the temperature in the body force term is considered to be linear based on

Boussinesq's model. Moreover, dissipation and pressure work are ignored in the present study. Under the above assumptions the governing equations of continuity, momentum, energy, and volume fraction are as follows [9]:

Continuity equation:

$$\nabla \cdot \mathbf{V} = 0 \tag{1}$$

Momentum equation:

$$\rho_{nf} \mathbf{V} \cdot \nabla \mathbf{V} = -\nabla p + \nabla \cdot \left((\mu_{nf} + \rho_{nf} \nu_t) \nabla \mathbf{V} \right) + (\rho \beta)_{nf} (T - T_c) \mathbf{g} \tag{2}$$

where \mathbf{V} is the mean flow velocity vector and \mathbf{g} is the gravitational acceleration vector i.e., $\mathbf{g} = -g\hat{i}$.

In the above equations ρ_{nf} , μ_{nf} , $\nu_{nf} = \left(\frac{\mu_{nf}}{\rho_{nf}} \right)$, ν_t and β_{nf} denote the density, the effective dynamic viscosity, effective kinematic viscosity, turbulent kinematic viscosity, and thermal expansion coefficient of nanofluid, respectively; T and p denote mean temperature and pressure fields.

Energy equation:

$$\left(\rho C_p \right)_{nf} \mathbf{V} \cdot \nabla T = \nabla \cdot \left(\left(\rho C_p \right)_{nf} \left(\frac{k_{nf}}{\left(\rho C_p \right)_{nf}} + \frac{\nu_t}{Pr_t} \right) \nabla T \right) - C_{p,p} \mathbf{J} \cdot \nabla T \tag{3}$$

Volume fraction equation:

$$\mathbf{V} \cdot \nabla \phi = -\frac{1}{\rho_p} \nabla \cdot (\mathbf{J}) \tag{4}$$

wherein Eqs. (3) and (4) k_{nf} , $C_{p,nf}$, $C_{p,p}$, Pr_t and ρ_p are nanofluid thermal conductivity, nanofluid heat capacity, particle heat capacity, turbulent Prandtl number, and particle density, respectively; ϕ is the local mean volume fraction of nanoparticles and \mathbf{J} is the nanoparticles mass flux. A Standard two-phase model of Buongiorno was presented for nanoparticle dispersion into the laminar flow of nanofluid, and in this model, the effect of nanoparticle diffusion due to turbulent eddies is not considered. Therefore, in this paper, Buongiorno's model is modified for considering the mass diffusion via turbulent eddies. Based on the presented modified Buongiorno's model nanoparticles mass flux can be written as:

$$\mathbf{J} = \mathbf{J}_B + \mathbf{J}_T + \mathbf{J}_{B, Turb} \tag{5}$$

\mathbf{J}_B , \mathbf{J}_T and $\mathbf{J}_{B, Turb}$ on right-hand side of Eq. (5) are mass flux due to Brownian motion, thermophoresis effect, and turbulent flow eddies, respectively.

\mathbf{J}_B is the drift flux due to the Brownian motion defined as [9]:

$$\mathbf{J}_B = -\rho_p D_B \nabla \phi \tag{6}$$

where the Brownian diffusion coefficient, D_B , is given by the Einstein-Stokes's equation:

$$D_B = \frac{K_B T}{3\pi\mu_f d_p} \tag{7}$$

\mathbf{J}_T is drift flux due to thermophoretic effects which can be defined as:

$$\mathbf{J}_T = -\rho_p D_T \frac{\nabla T}{T} \tag{8}$$

where D_T is thermophoresis coefficient which can be approximated as [11]:

$$D_T = \lambda \frac{\mu_f}{\rho_f} \phi \tag{9}$$

In Eq. (9), λ is a constant defined as $\lambda = 0.26 \frac{k_f}{k_f + k_p}$. λ is based on data for relatively large particles (1 micrometer) in water and n-hexane [11]. More accurate relationship may be found for the nanoparticles in the literature.

Moreover, the motion of nanoparticles within the base fluid due to the turbulent flow eddies ($\mathbf{J}_{B, Turb}$) could be defined as:

$$\mathbf{J}_{B, Turb} = -\rho_p D_{B, turb} \nabla \phi \tag{10}$$

where the turbulent diffusion coefficient $D_{B, turb}$ can be calculated as:

$$D_{B, turb} = \frac{\nu_t}{Sc_t} \tag{11}$$

In Eq. (11) Sc_t is the turbulent Schmidt number.

By substitution of Eqs. (6), (8) and (10) into Eq. (4), the closed form of volume fraction equation would be as:

$$\rho_p \mathbf{V} \cdot \nabla \phi = \nabla \cdot \left(\rho_p \left(D_B + \frac{\nu_t}{Sc_t} \right) \nabla \phi \right) + \nabla \cdot \left(\rho_p D_T \frac{\nabla T}{T} \right) \tag{12}$$

By considering the no-slip condition and zero mass flux of nanoparticles at the walls, the boundary conditions for Eqs. (1) to (3) and (12) would be as follows [12, 13]:

$$\begin{aligned} \mathbf{V} = \mathbf{0}, \nabla T \cdot \mathbf{n} = \nabla \phi \cdot \mathbf{n} = \mathbf{0} \text{ on the top and bottom walls} \\ \mathbf{V} = \mathbf{0}, T = T_h \text{ and } \nabla \phi \cdot \mathbf{n} = -\frac{D_T}{T} \nabla T \cdot \mathbf{n} \text{ on the left wall} \\ \mathbf{V} = \mathbf{0}, T = T_c \text{ and } \nabla \phi \cdot \mathbf{n} = -\frac{D_T}{D_B} \nabla T \cdot \mathbf{n} \text{ on the right wall} \end{aligned} \tag{13}$$

where \mathbf{n} is a unit vector normal to walls.

Table 1. Thermo-physical properties of water and nanoparticles at T = 310 K [25].

	$\rho(\frac{\text{kg}}{\text{m}^3})$	k(W/mK)	$C_p(\text{J/kgK})$	$\beta \times 10^5(\frac{1}{\text{K}})$	$\mu \times 10^6(\frac{\text{kg}}{\text{ms}})$	$d_p(\text{nm})$
Al ₂ O ₃	3970	40	765	0.85	-	13, 23, 33
Water	993	0.628	4178	36.2	695	0.385

2.3 Nanofluid properties

In this paper the nanofluid effective density ρ_{nf} , the heat capacity ($C_{p,nf}$) and the thermal expansion coefficient (β_{nf}) are obtained by these well-known formulas [23]:

$$\rho_{nf} = (1 - \phi)\rho_f + \phi\rho_p \tag{14}$$

$$(\rho C_p)_{nf} = (1 - \phi)(\rho C_p)_f + \phi(\rho C_p)_p \tag{15}$$

$$(\rho\beta)_{nf} = (1 - \phi)(\rho\beta)_f + \phi(\rho\beta)_p \tag{16}$$

where subscripts “f”, “p”, and “nf” refer to fluid, particle, and nanofluid, respectively.

Unfortunately, there is great ambiguity concerning the viscosity and the thermal conductivity of nanofluids. It is well accepted that these properties are influenced by many factors. Therefore, new and modified correlations for these quantities are constantly being published in the literature. By means of regression analysis of different experimental data Corcione [12,13] obtained empirical correlations for viscosity and thermal conductivity of nanofluids. The effect of important parameters such as temperature and particle size was considered in his formulas therefore, these correlations are frequently used in recently published papers [25-28].

Moreover, experimental results of Ghanbarpour et al. [29] confirm the validity of Corcione correlations. Therefore, these formulas are used in the present study which are as follows [25]:

$$\mu_{nf} = \mu_f / \left(1 - 34.87 \left(\frac{d_p}{d_f} \right)^{-0.3} \phi^{1.03} \right) \tag{17}$$

where d_p denote the diameter of nanoparticles (given in Table 1) and d_f is the base fluid molecules diameter (for water $d_f = 0.385 \text{ nm}$).

$$k_{nf} = k_f \left(1 + 4.4 (Re_B)^{0.4} Pr^{0.66} \left(\frac{T}{T_{fr}} \right)^{10} \left(\frac{k_p}{k_f} \right)^{0.03} \phi^{0.66} \right) \tag{18}$$

$$Re_B = \rho_f u_B d_p / \mu_f \tag{19}$$

$$u_B = 2K_B T / (\pi \mu_f d_p^2) \tag{20}$$

In the above equations, T_{fr} , u_B and K_B refer to the freezing point of the base fluid, nanoparticle Brownian velocity, and Boltzmann’s coefficient ($K_B = 1.380648 \times 10^{-23} \text{ J/K}$), respectively.

Thermo-physical properties of water and nanoparticles are summarized in Table 1.

2.4 Non-dimensional form of governing equations

The following variables are introduced to non-dimensionalization of Eqs. (1) to (3) and (12):

$$\begin{aligned} x^* &= \frac{x}{H}, y^* = \frac{y}{H}, \nabla^* = H \nabla, \mathbf{V}^* = \frac{\mathbf{V}H}{\nu_f}, p^* = \frac{pH^2}{\rho_{nf} \nu_f^2}, T^* = \frac{T - T_c}{T_h - T_c}, \varphi^* = \frac{\varphi}{\varphi_{Ave}}, D_B^* = \frac{D_B}{D_{B0}}, D_{B,turb}^* = \frac{D_{B,turb}}{D_{B0}}, D_T^* = \frac{D_T}{D_{T0}}, \delta = \frac{T_c}{T_h - T_c}, \\ Ra &= \frac{g \beta_f (T_h - T_c) H^3}{\alpha_f \nu_f}, Pr = \frac{\nu_f}{\alpha_f} \end{aligned}$$

where, $D_{T0} = \gamma \frac{\mu_f}{\rho_f} \varphi_{ave}$, $D_{B0} = \frac{k_B T_c}{3\pi \mu_f d_p}$ and $\alpha_f = \frac{k_f}{(\rho C_p)_f}$

The dimensionless form of governing equations could be written as below.

Non-dimensional form of continuity equation:

$$\nabla^* \cdot \mathbf{V}^* = 0 \tag{21}$$

dimensionless momentum equation:

$$\begin{aligned} \left(\frac{\rho_{nf}}{\rho_f} \right) \mathbf{V}^* \cdot \nabla^* \mathbf{V}^* &= - \left(\frac{\rho_{nf}}{\rho_f} \right) \nabla^* p^* + \\ \nabla^* \cdot \left[\left(\frac{\mu_{nf}}{\mu_f} + \frac{\rho_{nf} \nu_t}{\mu_f} \right) \nabla^* \mathbf{V}^* \right] &+ \\ \left[\left(\frac{\rho\beta}{\rho_f \beta_f} \right) \cdot \frac{1}{Pr} Ra T^* \right] \mathbf{e}_g & \end{aligned} \tag{22}$$

where $\mathbf{e}_g = \frac{\mathbf{g}}{|\mathbf{g}|}$ is a unit vector of gravitational acceleration. Non-dimensional energy equation:

$$\begin{aligned} \left(\frac{\rho C_p}{\rho_f c_{p,f}} \right) \mathbf{V}^* \cdot \nabla^* T^* &= \frac{1}{Pr} \nabla^* \cdot \left[\left(\frac{k_{nf}}{k_f} \right) \nabla^* T^* \right] + \\ \frac{1}{Pr} \cdot \frac{1}{Le} \left\{ \frac{(D_B^* + D_{B,turb}^*) \nabla^* \varphi^* \cdot \nabla^* T^*}{N_{BT}} + \frac{D_T^* \nabla^* T^* \cdot \nabla^* T^*}{1 + \delta T^*} \right\} & \end{aligned} \tag{23}$$

And the dimensionless form of volume fraction equation:

$$V^* \cdot \nabla^* \varphi^* = \frac{1}{Sc} \nabla^* \cdot \left[(D_B^* + D_{B,turb}^*) \nabla^* \varphi^* + \frac{1}{N_{BT}} \cdot \frac{D_T^*}{1 + \delta T^*} \nabla^* T^* \right] \quad (24)$$

In the above equations, $Sc = \frac{\nu_f}{D_{B0}}$, $N_{BT} = \frac{\varphi_{ave} D_{B0} T_c}{D_{T0} (T_h - T_c)}$ and $Le = \frac{k_f}{\rho_p c_p \varphi_{ave} D_{B0}}$ represent Schmidt number, diffusivity ratio parameter (Brownian diffusivity/thermophoretic diffusivity), and Lewis number, respectively [9].

The dimensionless form of boundary conditions can be written as:

$$\begin{aligned} V^* = 0, \nabla^* T^* \cdot \mathbf{n} = \nabla^* \varphi^* \cdot \mathbf{n} = 0 \text{ and on the top and bottom walls} \\ V^* = 0, T^* = 1 \text{ and } \nabla^* \varphi^* \cdot \mathbf{n} = -\frac{D_T^*}{D_B^*} \cdot \frac{1}{N_{BT}} \cdot \frac{1}{1 + \delta T^*} \nabla^* T^* \cdot \mathbf{n} \text{ on the left wall} \quad (25) \\ V^* = 0, T^* = 0 \text{ and } \nabla^* \varphi^* \cdot \mathbf{n} = -\frac{D_T^*}{D_B^*} \cdot \frac{1}{N_{BT}} \cdot \frac{1}{1 + \delta T^*} \nabla^* T^* \cdot \mathbf{n} \text{ on the right wall} \end{aligned}$$

The average Nusselt number is calculated by integrating the local Nusselt number along the hot vertical wall of the cavity.

$$Nu_{Ave} = -\int \frac{k_{nf}}{k_f} \nabla^* T^* \cdot \mathbf{n} \, dy^* \quad (26)$$

2.5 $v^2 - f$ turbulence model

In the standard $K - \varepsilon$ turbulence model, the Boussinesq assumption is utilized. In the near-wall region the Standard $K - \varepsilon$ turbulence model must be modified by damping functions. These functions are derived for benchmark turbulent flows, such as channel flows, and are not suited for complex turbulent flows. Durbin [30] introduced an eddy viscosity formulation, $v^2 - f$ turbulence model, which uses a turbulent wall-normal stress component v^2 . This turbulent normal stress component is considered as the turbulent velocity scale ($v^2 = v'^2$). In the $v^2 - f$ model, the turbulent viscosity can be calculated as follows:

$$\nu_t = c_\mu \overline{v^2} \tau \quad (27)$$

where c_μ is constant value and τ is the turbulent time scale. The $v^2 - f$ model suggested by Durbin [30-32] was numerically unstable using pressure correction method-based segregated solvers. To make the $v^2 - f$ model suitable for segregated solvers or for incompressible flow simulations Lien and Kalitzin [33] modified the model. So that it becomes much more numerically stable. The modified $v^2 - f$ turbulence model can be written as follow:

$$u_j \frac{\partial \overline{v^2}}{\partial x_j} = -6 \frac{\overline{v^2}}{K} \varepsilon + Kf + \frac{\partial}{\partial x_j} \left((v_{nf} + \frac{v_t}{\sigma_k}) \frac{\partial \overline{v^2}}{\partial x_j} \right) \quad (28)$$

$$\frac{\partial}{\partial x_j} \left((v_{nf} + \frac{v_t}{\sigma_k}) \frac{\partial \overline{v^2}}{\partial x_j} \right)$$

$$\begin{aligned} L^2 \frac{\partial^2 f}{\partial x_j \partial x_j} - f = \frac{C_1}{\tau} \left(\frac{\overline{v^2}}{K} - \frac{2}{3} \right) - \\ C_2 \frac{P_k}{K} - \frac{1}{\tau} \left(6 \frac{\overline{v^2}}{K} - \frac{2}{3} \right) \end{aligned} \quad (29)$$

where u_j , $K = \frac{1}{2} (\overline{u'_i u'_i})$ and $P_k = 2 C_\mu \overline{v^2} \tau S_{ij} S_{ij}$ are mean flow velocity components, turbulent kinetic energy, and production of turbulent kinetic energy, respectively. Moreover, u'_j and $S_{ij} = \frac{1}{2} \left(\frac{\partial u_i}{\partial x_j} + \frac{\partial u_j}{\partial x_i} \right)$ demonstrated the velocity fluctuation components and strain rate tensor. It turns out that in the region far away from the wall $\frac{\overline{v^2}}{v^2}$ gets too large so that $\frac{\overline{v^2}}{v^2} > \frac{2}{3} K$. For this reasons Sveningsson et al. [34] proposed a modification to set an upper limit for the source term kf in the $\frac{\overline{v^2}}{v^2}$ - equation as

$$\Phi_{v^2 f, source} = \min(Kf, \Pi_{kf}) \quad (30)$$

$$\Pi_{kf} = -\frac{1}{\tau} \left[(C_1 - 6) \overline{v^2} - \frac{2}{3} K (C_1 - 1) \right] + C_2 P_k \quad (31)$$

This modification ensures that $\frac{\overline{v^2}}{v^2} < \frac{2}{3} K$. On the other hand, in regions where $\frac{\overline{v^2}}{v^2} < \frac{2}{3} K$ the $v^2 - f$ model predicts the turbulent viscosity considerably larger than the standard $K - \varepsilon$ turbulence model so that Sveningsson et al. [34] suggested a simple modification to compute the turbulent viscosity:

$$\nu_t = \min \left(c_\mu \overline{v^2} \tau, c_\mu \frac{K^2}{\varepsilon} \right) \quad (32)$$

The $v^2 - f$ model is based on the standard $K - \varepsilon$ model. Then, the turbulent time scale τ and length scale L are given by

$$\tau = \max \left(\frac{K}{\varepsilon}, 6 \sqrt{\frac{\overline{v^2}}{\varepsilon}} \right) \quad (33)$$

$$L = C_L \max \left(\frac{K^{3/2}}{\varepsilon}, C_\eta \frac{\overline{v^2}}{\varepsilon^{1/4}} \right) \quad (34)$$

K and ε are determined from the standard $K - \varepsilon$ equations:

$$u_j \frac{\partial K}{\partial x_j} = P_k - \varepsilon + \frac{\partial}{\partial x_j} \left((v_{nf} + \frac{v_t}{\sigma_k}) \frac{\partial K}{\partial x_j} \right) \quad (35)$$

$$u_j \frac{\partial \varepsilon}{\partial x_j} = \frac{C_{\varepsilon 1} P_k - C_{\varepsilon 2} \varepsilon}{\tau} + \frac{\partial}{\partial x_j} \left((v_{nf} + \frac{v_t}{\sigma_\varepsilon}) \frac{\partial \varepsilon}{\partial x_j} \right) \quad (36)$$

In the current work the model constants for the $v^2 - f$ and standard $K - \varepsilon$ turbulence model are given as Table 2:

Table 2. and standard turbulence model constants

C_μ	$C_{\varepsilon,1}$	$C_{\varepsilon,2}$	C_1	C_2	C_L	C_η	σ_k	σ_ε
0.22	1.4	1.9	1.4	0.3	0.23	70	1	1.3

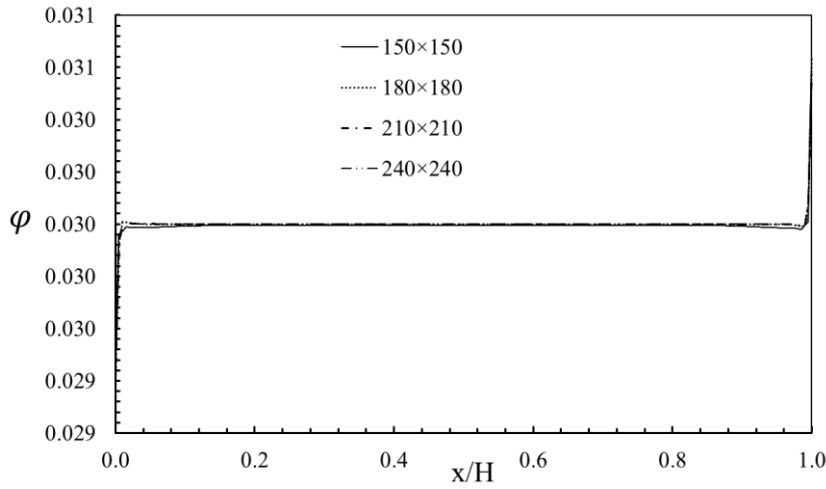


Fig. 2. Local volume fraction variation along the horizontal centerline of cavity ($y^*=0.5$) for $Pr=4.623, \phi_{Ave}=0.03$.

The wall boundary conditions for \overline{v}^2 and standard $K - \varepsilon$ turbulence models are as follow:

$$\overline{v}^2 = f = K = 0 \text{ and } \nabla \varepsilon \cdot \mathbf{n} = 0 \tag{37}$$

3- Numerical Method, Grid Study and Verification

The governing equations with the associated boundary conditions are numerically solved using the SIMPLE-based finite volume method on a co-located grid [35]. Diffusion terms in the governing equations are discretized using a second-order central difference scheme while an upwind scheme is used to discretize the convective terms. The thermo-physical properties such as density, viscosity, and thermal conductivity as well as thermophoresis diffusion and Brownian motion coefficients, which are varied with temperature and volume fraction, are obtained simultaneously with flow, temperature, and volume fraction equations in the whole domain. To obtain converged solutions, an under-relaxation coefficient of 0.5 is used for the momentum and the energy equations while the under-relaxation factor for volume fraction transport equation is set to 0.6.

3.1. Grid study

The numerical solution of governing equations shows that there is a sharp volume fraction gradient especially near the walls; thus, the results are sensitive to the number of grids. In this work, a structured mesh is used in simulations (Fig. 1 (b)). Fig. 2 shows the effect of the number of grids on the local nanoparticles distribution along the horizontal centerline of the cavity ($y^* = \frac{y}{H} = 0.5$). Moreover, the average Nusselt numbers obtained using different grid numbers are presented in Table 3. From Fig. 2 and Table 3, it is seen that by changing the grid numbers from 210x210 to 240x240, the

Table 3. Effect of the grid size on the average Nusselt number ($Ra=10^9, Pr=4.623, \phi_{Ave}=0.02$).

Grid	Nu_{Ave}
150 x 150	65.1885423
180 x 180	65.1914512
210 x 210	65.19433621
240 x 20	65.19542511

variation of nanoparticles local distribution and the average Nusselt number is not significant, thus a uniformly structured grid system of 210x210 is used for all simulations. Moreover, for this mesh number $y_c^+ = \frac{u_\tau y_c}{\nu_{nc}}$ (u_τ : friction velocity and y_c distance of cell center of first near-wall cell) of centers of all near-wall meshes are less than 1 ($y_c^+ < 1$). Therefore, in this work wall functions are not utilized as boundary conditions.

3.2. Code validation

For validation of two-phase flow modeling part of code, laminar natural convection of Al_2O_3 -water nanofluid inside a square cavity for $d_p=33$ nm, $2 \leq \Delta T \leq 10$ ($3.37 \times 10^5 \leq Ra \leq 1.68 \times 10^6$), the average volume fraction of 3% ($\phi_{ave} = 0.03$) and $Pr=4.623$ is used. Both experimental (Ho et al. [36]) and numerical results (Sheikhzadeh et al.[15] and Garoosi et al. [16]) are available for this benchmark case. It should be noted that in the above-mentioned numerical studies Buongiorno’s mathematical model for laminar flow was used. Comparison of the average Nu number as a function of Ra number is depicted in Fig.3. In general, there is a good agreement between the present results and the results of reference [36]. The difference between the numerical and

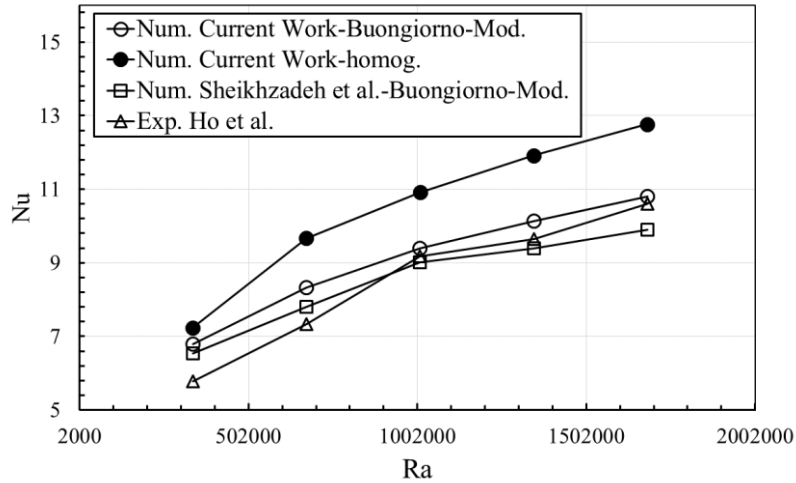


Fig. 3. Comparison of the mean Nusselt number obtained from present numerical simulation with the experimental results of Ho et al. [36] and numerical results of Sheikhzadeh et al. [15] at different Ra numbers.

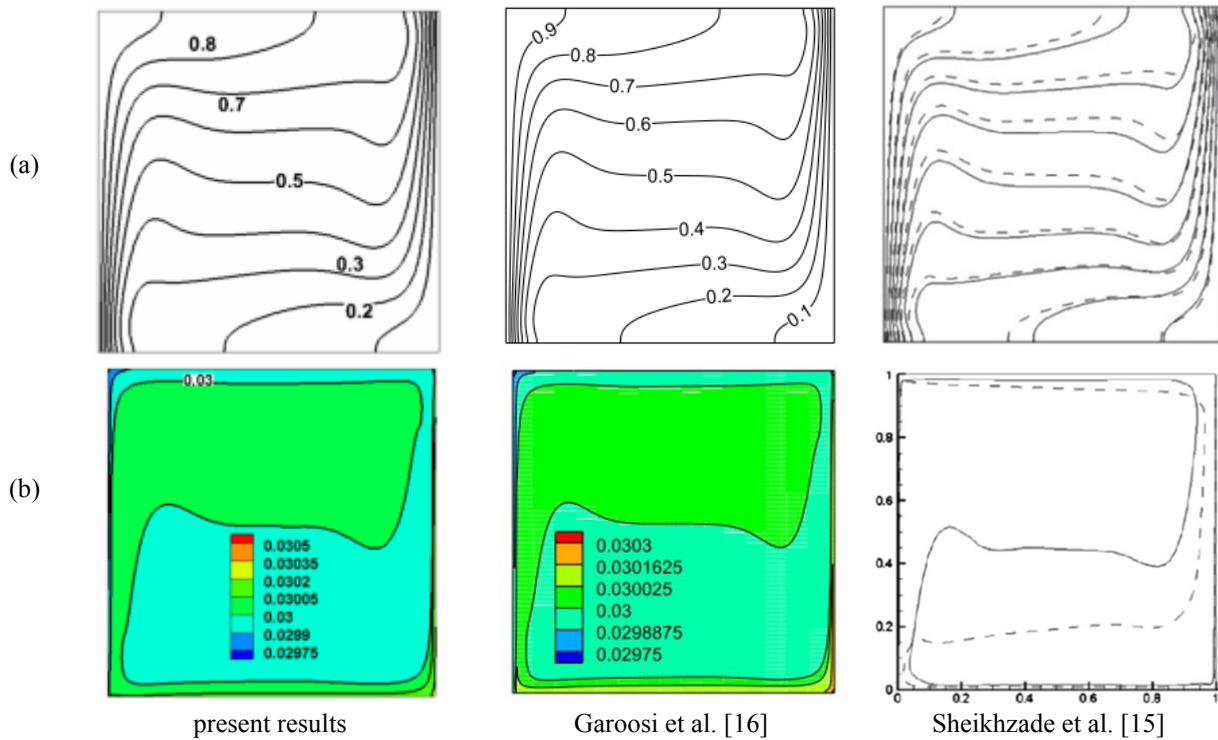


Fig. 4. Comparison of present results with the numerical results of Sheikhzade et al. [15] and Garoosi et al. [16] (a) isotherms and (b) contours of nanoparticles distribution.

laboratory results can be for the following error sources: the errors related to measurement instruments, uncertainty and repeatability of reference experimental results, and the modeling errors, truncation, iteration (error caused because of iteration process to solve the linear equation system) and round off errors. More accurate physical and mathematical models, for modeling the nanofluid conductivity, nanofluid viscosity, turbulence, and stable high-order numerical methods can be used to improve the computational accuracy. Furthermore, It can be seen that the results of the two-phase Buongiorno model are closer to the experimental results

rather than homogeneous single-phase simulation because of considering the effects of migration of nanoparticles in base flow due to the thermophoresis effect. However, as mentioned in the original work of Buongiorno [11], in Eq. (9), \tilde{c} is a constant defined as $\lambda = 0.26 \frac{k_f}{k_f + k_p}$. \tilde{c} is based on data for relatively large particles (1 micrometer) in water and n-hexane [11]. Certainly, using more accurate models to calculate \tilde{c} can improve results.

In addition, isotherms and nanoparticle distribution obtained from the present work are compared with the results of references [15, 16] in Fig. 4. As shown in Figs. 4 the present

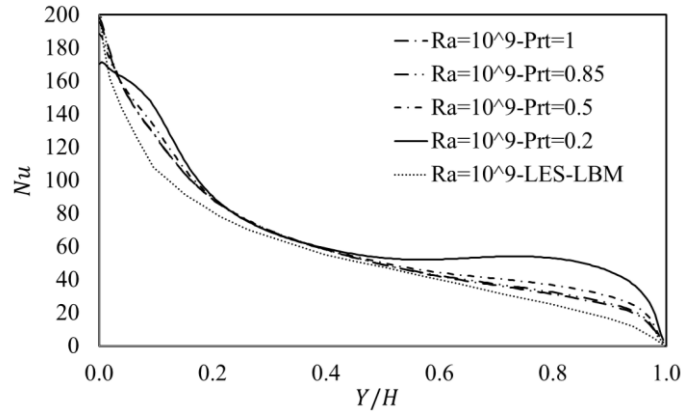


Fig. 5. Variation of local Nu number at $Ra=10^9$ for different Pr_t numbers (current work) and LES-LBM method [24]

Table 4 Comparison of the turbulent solution with previous works (mean Nu at high Ra -values)

Ra	Nu_{Ave} (current work)	Nu_{Ave} Sajjadi et al. [24]	Nu_{Ave} Barakos et al. [39]	Nu_{Ave} Henkes et al. [37]	Nu_{Ave} Markatos et al. [38]
10^7	17.45154621	17.569	-	-	-
10^8	32.61228289	35.268	32.3	32.5	32.05
10^9	62.79671401	57.939	60.1	59.5	74.7

results are in close agreement with other numerical studies.

For validation of turbulent modeling part of code and setting the magnitude of turbulent Prandtl number, distribution of local Nu number along the hot wall for different turbulent Prandtl numbers ($Pr_t=0.2, 0.5, 0.85$ and 1) are compared with results of Lattice Boltzmann Method based on Large Eddy Simulation model (LES-LBM) of reference [24] at $Ra=10^9$ for pure water.

It can be seen that results of $Pr_t = 0.85$ and 1 are closer to the LES. In the present work, Pr_t of 0.85 is used for simulations. Furthermore, for the turbulent case, Table 4 presents a comparison of current results for the average Nu with results by Sajjadi et al. [24], Henkes et al. [37], Markatos et al. [38], and Barakos et al. [39]. For $Ra = 10^7$ and 10^8 the all available solutions agree remarkably well. As Ra increases ($Ra=10^9$), present results show good agreement with the other solutions, while Markatos and Pericleous give somewhat higher values.

4- Results and Discussion

Turbulent natural convection of Al_2O_3 -water nanofluid in a square cavity is simulated by using modified Buongiorno’s model with considering the effect of thermophoresis, Brownian, and turbulence on the motion of nanoparticles. Computations are performed at the following values of non-dimensional parameters: Rayleigh numbers ($Ra=10^7, Ra=10^8$ and $Ra=10^9$), average particle volume fractions ($0 \leq \phi_{Ave} \leq 0.04$), and Lewis number ($2.62 \times 10^5 \leq Le \leq 1.05 \times 10^6$). In all cases, the values of δ , Pr, Sc, and N_{BT} are fixed at $155, 4.623, 3.55 \times 10^4$ and 1.1 , respectively.

The effects of above-mentioned parameters on flow

structure, nanoparticle local distribution, turbulent kinetic energy, turbulent intensity, and heat transfer are presented in the following sections.

4.1. Effects of Ra number on flow pattern, temperature field, and nanoparticle distribution

Figs. 6 (a) and (b) depict the isotherms (left column), streamlines (central column), and iso-concentration line of $\phi = 0.02$ (right column) of water- Al_2O_3 nanofluid over a turbulent regime ($Ra = 10^8$ and 10^9). In high Rayleigh numbers, replacing conduction, advection becomes the predominant heat transfer mechanism. Accordingly, the isotherms emerge horizontally in the cavity except in the neighborhood of the vertical wall boundaries. Moreover, there appears clear stratification of isotherms along the vertical direction within almost the whole domain except the very thin layers attached to the vertical walls. These thin layers could be seen in Fig. 6 (c). Fig 6 (c) illustrates the non-dimensional temperature distribution (T^*) on the horizontal centerline of the cavity for the conditions of ($\phi = 0.02, d_p = 33nm$, and $Ra=10^8$ and 10^9).

The patterns of streamlines of mean-flow are asymmetric. A vortex has formed in the core region and there are two vortices surrounding it. The central vortex expands quickly with the Rayleigh number enhancing ($Ra=10^9$). As shown by these plots, for turbulent natural convection of nanofluid within a square cavity, the patterns of isotherms are always different from that of iso-concentrations. It is seen that at $Ra=10^8$ a mass boundary layer exists close to all walls. The patterns of iso-concentrations are strictly symmetric with respect to the center of the square cavity. On the other hand, with increasing

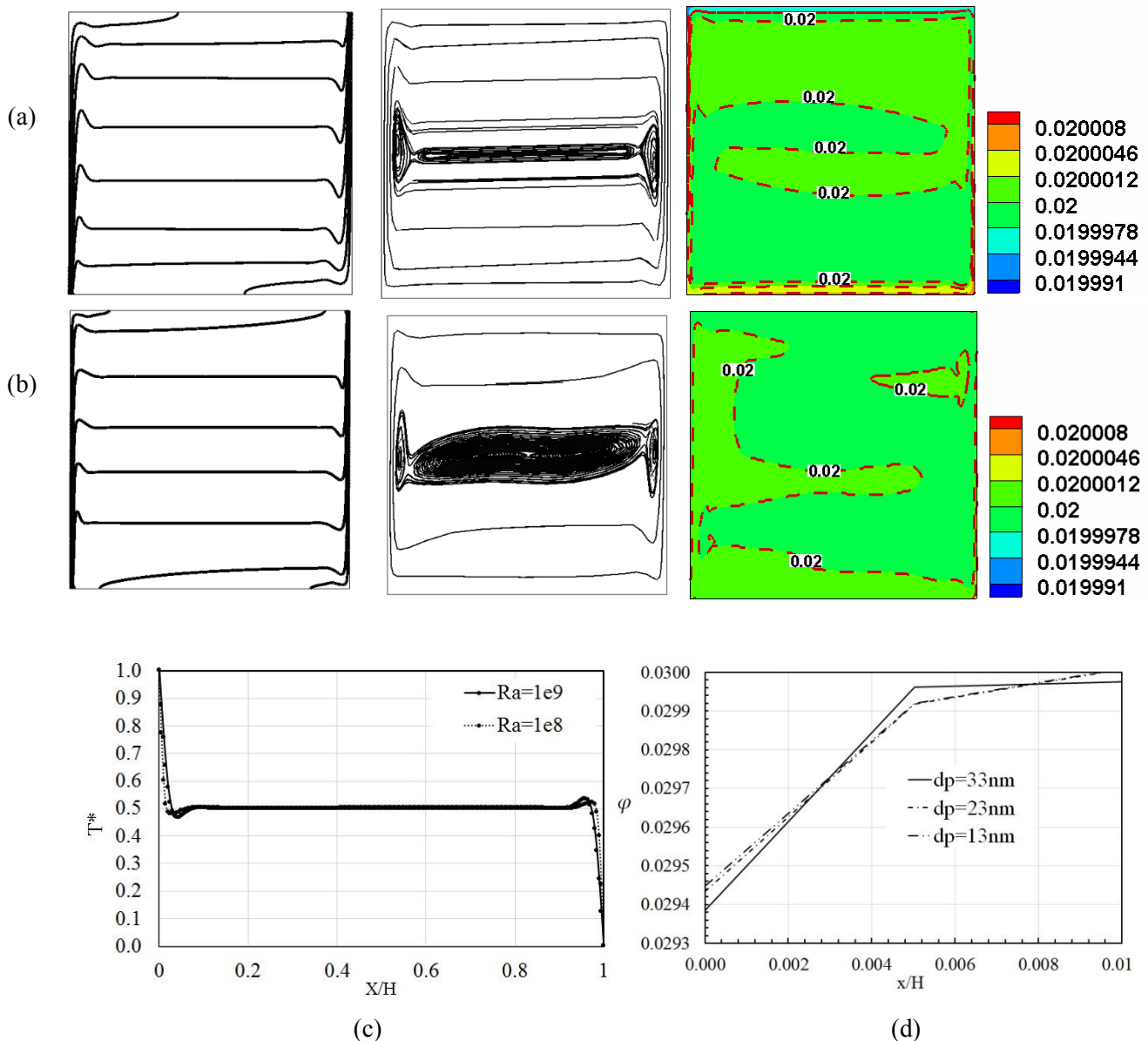


Fig. 6. Isotherms (left column), streamlines (central column) and iso-concentration line (right column) of , for (a) $Ra=10^8$ (b) $Ra=10^9$ (c) non-dimensional temperature distribution on horizontal centerline of cavity (and $d_p=33\text{nm}$) and (d) local distribution of volume fraction for different nanoparticle diameters ($Ra=10^9$ and)

Ra , the distribution of the solid particles becomes uniform. This is because an increase in Ra results in higher advection intensity and the size of the main circulation is also increased so that more particles are trapped in the recirculating area and less deposition is expected. Thus, the distribution of particles becomes almost uniform. Another observation is that the particle concentration near the cold wall is higher than at the hot wall. This can be related to thermophoretic effects when the temperature gradient transports the particles from hot to cold regions. It will be shown that (in section 4.4) the mass flux due to the thermophoresis effect is stronger than other slip mechanisms even in turbulent flow near the hot and cold walls.

Local distribution of volume fraction for different nanoparticle diameters of $d_p=13, 23,$ and 33 nm and at

conditions of ($Ra=10^9$ and $\delta = 0.03$) are demonstrated in Fig. 6 (d), in near hot wall region ($X/H < 0.01$). Basically, according to Eq. (7), the Brownian diffusion coefficient decreases with the increasing diameter of the nanoparticles, thus the nanoparticle penetration is reduced due to the Brownian effect and the thermophoresis effects become stronger. Because of this, the local volume fraction of particles decreases near the hot wall with increasing the particles diameter, Fig. 6 (d).

4.2. Effect of average volume fraction and Ra number on Average Nu number

In Fig. 7, the variation of the average Nu number of the hot wall versus the particle volume fraction is displayed for different Ra numbers. According to Fig. 7, for all Ra numbers, there is an optimum value of particles' average volume fraction

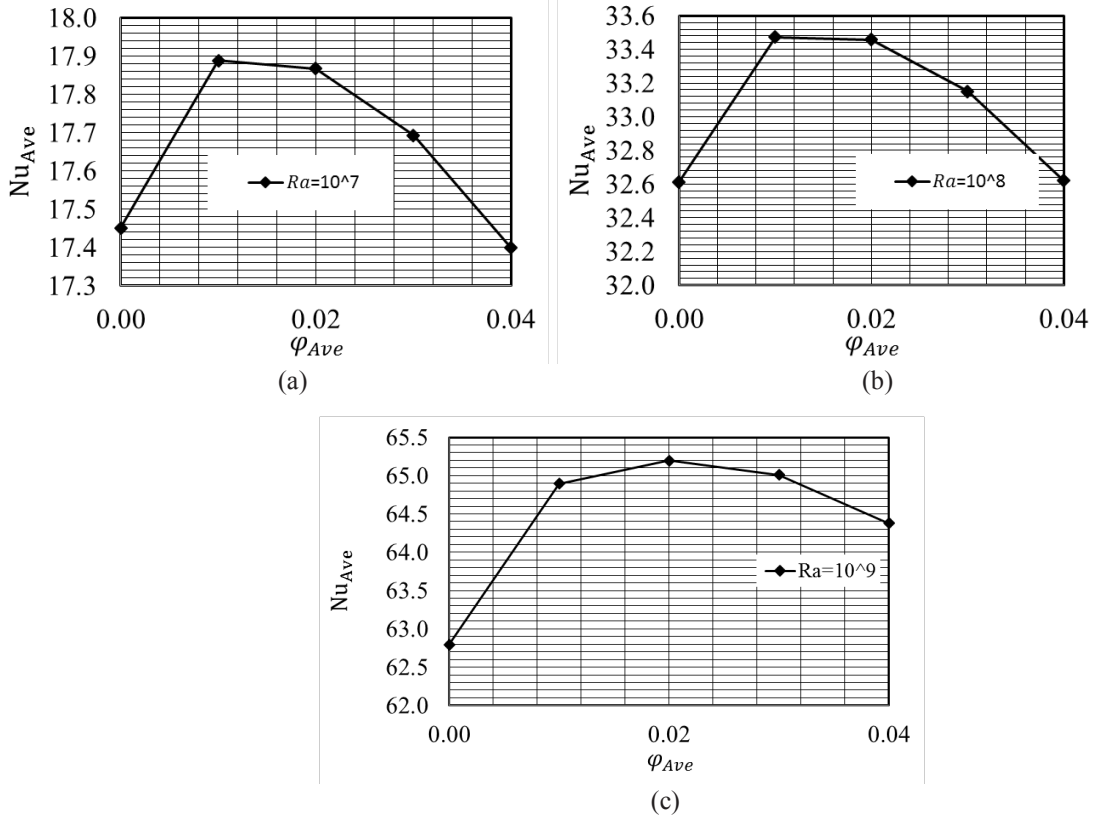


Fig. 7. Variation of the average Nu number versus the average particle volume fraction for (a) $Ra=10^7$, (b) $Ra=10^8$ and (c) $Ra=10^9$.

(ϕ_{opt}) which the maximum heat transfer rate occurs there. It is an interesting observation. It may be related to the existence of two conflicting effects. Increasing the nanoparticle volume fraction causes an enhancement in both viscosity and thermal conductivity of the fluid. Consequently, with increasing the viscosity, the thickness of the thermal boundary layer is increased and hence the temperature gradient near the hot and cold walls is decreased leading to lower heat transfer rates. For $\phi_{Ave} > \phi_{opt}$, the negative effect of viscosity rise on boundary layer is stronger than the positive effects of thermal conductivity enhancement and thus heat transfer rate is decreased. Based on Fig.7, the optimum particle volume fractions are 1% for $Ra=10^7$, 10^8 and 2% for $Ra=10^9$. Similar trends are reported for laminar flows at high Ra numbers in reference [19]. Our results demonstrate this conclusion is still valid beyond laminar regimes.

4.3. Effect of nanoparticles on turbulence characteristics

Fig. 8(a) shows the turbulent kinetic energy, K (m^2/s^2), color contours at the highest studied Ra number ($Ra=10^9$) for the average nanoparticles volume fraction of 2%. It can be seen that turbulent kinetic energy contours are symmetric with respect to the center of the square cavity and kinetic energy is maximum near the top-left corner ($Y=0.75$) and bottom-right corner ($Y=0.25$) of the cavity. The magnitude of the highest turbulence kinetic energy is 3.14×10^{-4} .

Fig. 8(b) and (c) illustrate the model predictions for the turbulence intensity profiles at line 1($Y=0.75$) and 2($Y=0.5$)

(shown on Fig. 8 (a)), respectively. Turbulence intensity is defined as the ratio of root-mean-square fluctuation velocity to the buoyancy velocity scale $U_B = \sqrt{g\beta H(T_h - T_c)}$, that is:

$$TI(\%) = \frac{\sqrt{\frac{1}{3}(\overline{u'_j u'_j})}}{U_B} \times 100 = \frac{\sqrt{\frac{2}{3}K}}{U_B} \times 100 \quad (38)$$

As can be seen from the figures, generally, the magnitude of turbulence intensity inside the cavity is low. These figures additionally show that the minimum turbulence intensity value is zero, and they are located on the left and right walls. Furthermore, the maximum value occurs within the right wall's boundary layer over line 1. Moreover, when the nanoparticle volume fraction increases, turbulence intensity remains constant. Then, nanoparticles have no effect on turbulence intensity level inside the cavity at studied average volume fractions. Goodarzi et al. [40] have observed similar results.

4.4. Comparison among order of magnitude of nanoparticle fluxes of J_B , J_T and $J_{B,Turb}$

Figs. 9 (a), (b), and (c) illustrate the simulation results for the iso-concentration line of 0.02, streamlines, and isotherms of water- Al_2O_3 nanofluid at $Ra=10^9$ without $J_{B,turb}$ term in Eq. (5). According to Fig. 6 (b) and Fig. 9, it is evident that $J_{B,turb}$ has no significant effects on flow characteristics.

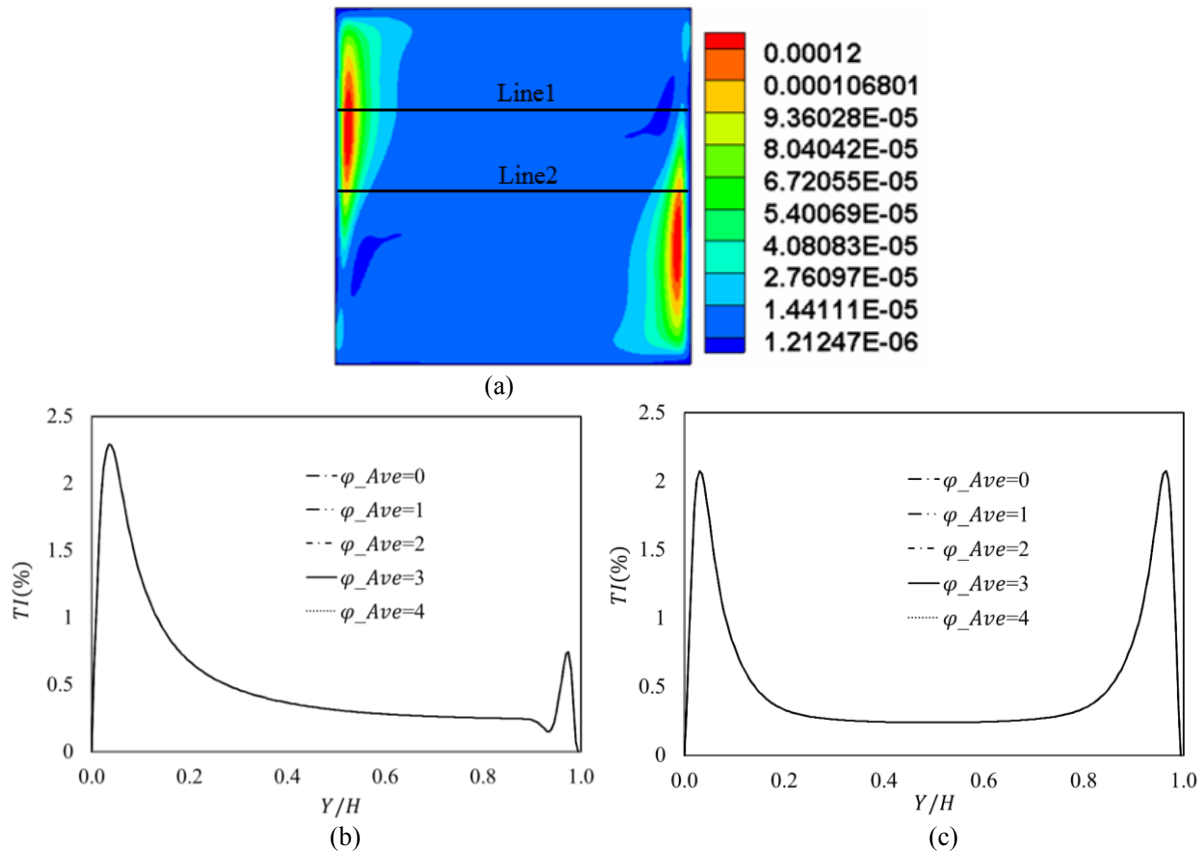


Fig. 8. Effect of nanoparticle average volume fraction on (a) turbulent kinetic energy colour contours in m^2/s^2 , (b) turbulence intensity distribution on line 1 ($Y = 0.75$), and (c) turbulence intensity distribution on line 2 ($Y = 0.5$) for $Ra=10^9$

In order to investigate the effect of the nanofluid modeling method (single-phase or two-phase) and the presence or absence of different terms of the equation of Buongiorno's two-phase models (Brownian J_B , thermophoresis J_T and turbulent diffusion $J_{B,Turb}$ terms) on the Nu_{ave} , the numerical solution results by four different methods are presented in Fig. 9 (d). In case 1, a single-phase homogeneous model is used to model the nanofluid properties. In case 2, only the Brownian term ($J=B$) and in case 3 both Brownian and thermophoresis terms ($J=J_B+J_T$) are considered in Buongiorno's model. Besides, in case 4, in addition to the Brownian and thermophoresis terms, the term of particle diffusion by turbulent eddies ($J=J_B+J_T+J_{B,Turb}$) are taken into account (modified Buongiorno model). Other parameters are same for all four cases as: $Ra=10^9$, $d_p=33nm$ and $\ddot{O} = 0.0, 0.01, 0.02, 0.03$ and 0.04 . By comparing the values obtained for the Nusselt number by the single-phase model (case 1) with the two-phase model of case 2 ($J=J_B$), the method of case 1 is predicted the Nusselt number up to 12% higher than the case 2 values. Furthermore, the method used in case 2 estimates the Nusselt number up to 4% more than the results of scheme of case 3 ($J=J_B+J_T$). Moreover, the results of case 3 are almost the same as those of case 4 ($J=J_B+J_T+J_{B,Turb}$). Therefore, based on the above, it can be concluded that the use of the two-phase model has a great effect on the solution results, and also considering the thermophoresis diffusion has a significant effect on the

Nusselt number prediction. In addition, the diffusion term caused by turbulent eddies does not have much effect on the prediction of heat transfer rate results.

For understanding this phenomenon, it may be necessary detailed study on the turbulent nanoparticles flux magnitude ($J_{p,B,turb} = -\rho_p D_{B,turb} \nabla \varphi$) inside the cavity flow. In Fig. 10 (a) color contours of turbulent diffusion coefficient ($D_{B,turb} = \frac{v_t}{Sc_t}$) are demonstrated. From the Figure, $D_{B,turb}$ is maximum near the top-left corner ($Y \approx 0.75$) and bottom-right corner ($Y \approx 0.25$) of the cavity. Profiles of variations of $D_{B,turb}$ and x-component of $\nabla \varphi$ near the hot wall ($0 < X/H < 0.1$) over line 1 ($Y=0.75$) are shown in Fig. 10 (b) and Fig. 10 (c). It is seen that $D_{B,turb}$ is zero on the wall and it is maximum in $X/H=0.05$ (or in buffer layer of the turbulent boundary layer); on the other hand, according to the Fig. 10 (c) x-component of $\nabla \varphi$ ($\frac{\partial \phi}{\partial x}$) is approached to the zero beyond the point of $X/H=0.01$ and would be approximately zero in $X/H=0.09$. In the other words, the border of the mass boundary layer is located at about $X/H=0.01$ (or inside the viscous sublayer of the turbulent boundary layer); therefore, the mass boundary is so thin and it is located inside the viscous sublayer. It means that the location of the maximum value of $D_{B,turb}$ is out of the mass boundary layer, then the magnitude of $J_{B,Turb,x} = -\rho_p D_{B,turb} \frac{\partial \phi}{\partial x}$ would be small inside the mass boundary layer. In Fig. 10 (d) values of the x-component of thermophoretic, Brownian, and turbulent nanoparticles flux are compared at line 1 ($Y=0.75$)

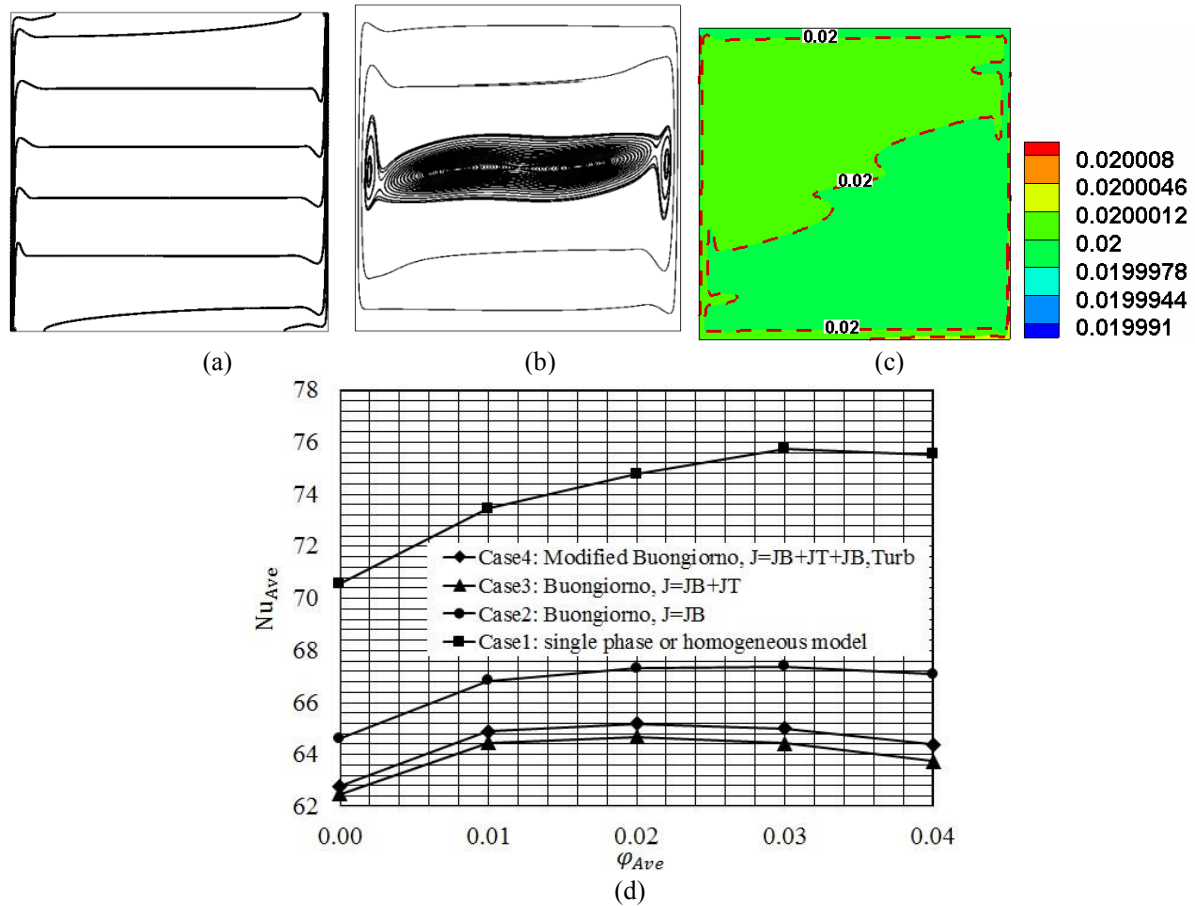


Fig. 9. (a) Isotherms (b) streamlines (c) iso-concentration line of for $Ra=10^9$ without $J_{B,turb}$ effect and (d) Nu_{ave} versus average volume fraction for different models

and $2(Y=0.5)$. It is clear that in regions far from the walls ($X/H > 0.09$) all fluxes tend to zero. Generally, it could be said that magnitude of turbulent flux is small in comparison with Brownian and thermophoretic flux even inside the mass boundary layer (for example at line 2, $Y=0.5$), and only in small regions of the cavity, which $D_{B,turb}$ is large, may be comparable with other fluxes (for instance at line, $Y=0.75$), see Fig. 10 (d). On the other hand, with increasing Ra , the distribution of the solid particles becomes uniform. This is because an increase in Ra results in higher advection intensity and the size of the main vortex inside the cavity is also increased so that more particles are trapped in the recirculating area and less deposition due to turbulent eddies is expected. Thus, the distribution of particles becomes almost uniform. Similar results have been observed in the laminar but high Rayleigh number in the work of Garoosi et al. [16].

4.5. Effect of values of Sc_t and Pr_t on average Nu number

The effect of Pr_t and Sc_t on Nu number are investigated in Fig. 11 at different average volume fractions for $Ra=10^9$.

From Fig. 11 (a) amount of Sc_t has a negligible effect on average Nu number values at all average volume fractions. It is because as it has been shown in section 4.5, the turbulent flux ($J_{b,turb}$) has low magnitude inside the cavity and has no

significant effect on flow pattern and temperature field. Furthermore, Fig. 11 (b) demonstrates that unlike the Sc_t , Pr_t has a significant effect on the Nu number magnitudes. With small Pr_t the numerical simulations predict high heat transfer rates. Moreover, the results obtained for $Pr_t = 0.85$ and 1 are close to each other.

5- Conclusions

In the current paper, the turbulent free convection of Al_2O_3 water nanofluid in a square enclosure was investigated. Two-phase Buongiorno's model was modified for considering the effect of diffusion due to the turbulent flow eddies. The effects of different parameters such as high Rayleigh numbers of ($10^7 \leq Ra \leq 10^9$), volume fraction ($0 \leq \phi_{Ave} \leq 0.04$), and turbulent Schmidt and Prandtl numbers on the heat transfer rate and distribution of nanoparticles are examined. The results of this research lead to the following conclusions:

-A proper validation with previous numerical investigations indicated that the RANS based v^2-f turbulence model is an appropriate method for turbulent and two-phase nanofluid flows problems.

-The effects of the nanoparticles volume fraction on turbulent kinetic energy and turbulence intensity are insignificant.

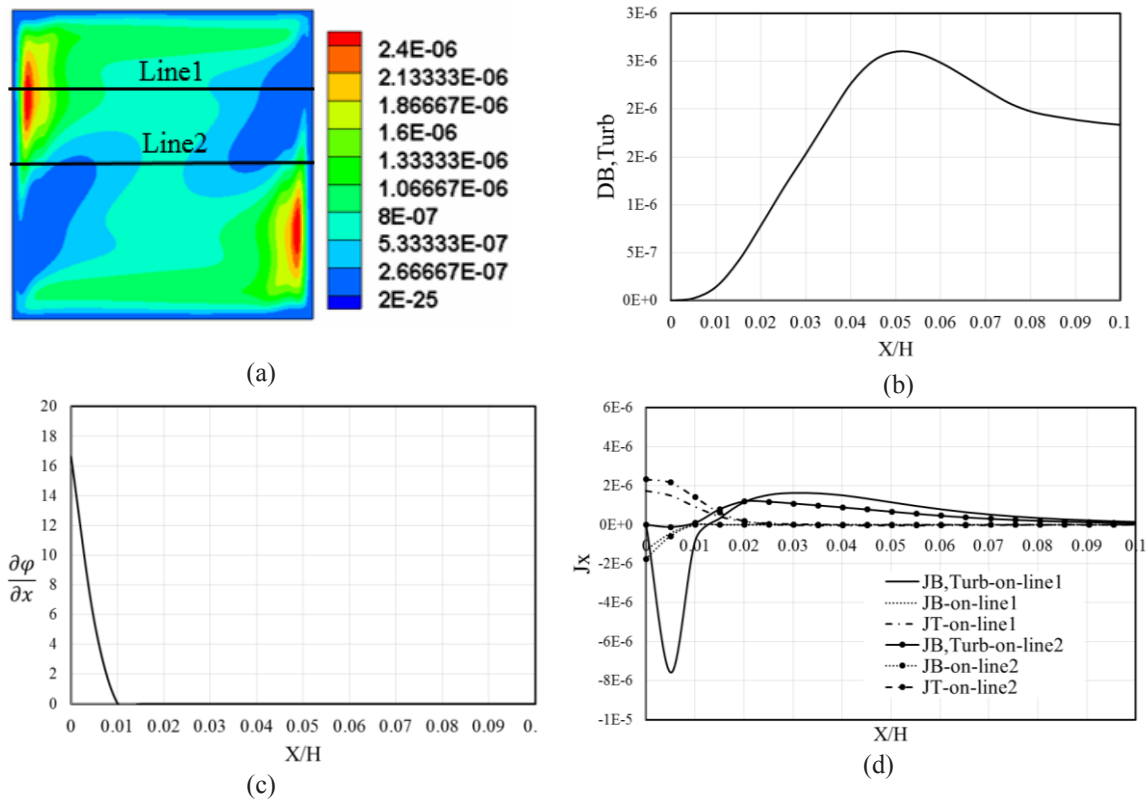


Fig. 10. (a) colour contours of turbulent diffusion $D_{B,Turb}$ coefficient, (b) $D_{B,Turb}$ variation at line 1 ($Y=0.75$), (c) variation at line 1 ($Y=0.75$) (d) x-component of Brownian flux (J_B), thermophoretic flux (J_T) and turbulent nanoparticle flux ($J_{B,Turb}$) at line 1 ($Y=0.75$) and at line 2 ($Y=0.5$).

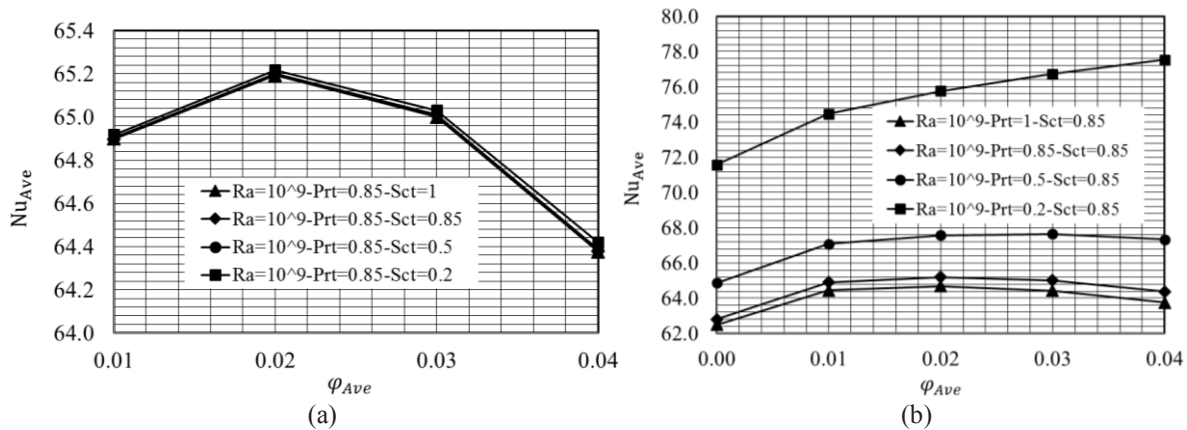


Fig. 11. Average Nu number versus average volume fraction for various (a) Sc_t and (b) Pr_t

-The magnitude of turbulent Schmidt had a negligible effect on the estimation of heat transfer rate. Against, low turbulent Prandtl numbers predicted higher values for the Nusselt number.

-At turbulent regimes where advection is strong, there are optimal average volume fractions with the maximum heat transfer rate depending on Ra number.

-From studied Ra numbers, at turbulent regimes, the particle distribution remains almost uniform.

-The nanoparticle diffusion flux due to the turbulent

eddies has no significant effects on heat transfer rate and nanoparticle distribution in investigated Ra numbers, based on the idea that the nanoparticles transfer boundary layer is so thin that it is fully encompassed in the viscous sub-layer of the turbulent fluid flow.

-For studied Ra numbers, related to turbulent flow, the thermophoresis effect is dominant at the near-wall regions similar to the laminar flow regimes.

The results presented in this research can answer some questions about the two-phase turbulent natural convection

of nanofluid inside the enclosure in detail and therefore accelerate the industrial application of nanofluid in the relevant fields.

NOMENCLATURES

C_p	specific heat, J kg ⁻¹ K ⁻¹
D_B	Brownian diffusion coefficient, kg m ⁻¹ s ⁻¹
D_{B0}	reference Brownian diffusion coefficient, kg m ⁻¹ s ⁻¹
$D_{B, turb}$	turbulent diffusion coefficient
d_f	diameter of the base fluid molecule, m
d_p	diameter of the nanoparticle, m
D_T	thermophoretic diffusivity coefficient, kg m ⁻¹ s ⁻¹
D_{T0}	reference thermophoretic diffusion coefficient, kg m ⁻¹ s ⁻¹
G	gravitational acceleration, ms ⁻²
H	height of cavity, m
J	particle flux vector, kg m ⁻² s ⁻¹
k	thermal conductivity, W m ⁻¹ K ⁻¹
K_B	Boltzmann's constant = 1.38066 × 10 ⁻²³ J K ⁻¹
K	Turbulence kinetic energy
Sc	Schmidt number
Sc_t	Turbulent Schmidt number
Le	Lewis number
N_{BT}	ratio of Brownian to thermophoretic diffusivity
Nu	Nusselt number
P	mean flow pressure, Pa
p^*	mean flow non-dimensional pressure
Pr	Prandtl number
Ra	Rayleigh number
Re_B	Brownian motion Reynolds number
T	mean flow temperature, K
T^*	mean flow dimensionless temperature
T_{fr}	freezing point of the base fluid, K
u_B	Brownian velocity of the nanoparticle, ms ⁻¹
V	mean flow velocity vector, ms ⁻¹
V^*	normalized mean flow velocity vector, ms ⁻¹
u_j	mean flow velocity components
u'_j	velocity fluctuation components
$\overline{v'^2}, v^2$	imaginary turbulent wall-normal stress component
x, y	Cartesian coordinates, m
x^*, y^*	dimensionless Cartesian coordinates
Greek symbols	
α	thermal diffusivity, m ² s ⁻¹
β	thermal expansion coefficient, K ⁻¹

Δ	normalized temperature parameter
λ	constant parameter
μ	dynamic viscosity, kg m ⁻¹ s ⁻¹
ν	kinematic viscosity, m ² s ⁻¹
ρ	density, kg m ⁻³
ϕ	volume fraction
ϕ^*	normalized volume fraction
Subscripts	
Ave	average
C	cold wall
H	hot wall
F	base fluid
P	particle
Nf	nanofluid
$Turb, t$	turbulence
T	thermophoresis
B	brownian

REFERENCES

- [1] G. Zhang, S.G. Kandlikar, A critical review of cooling techniques in proton exchange membrane fuel cell stacks, international journal of hydrogen energy, 37(3) (2012) 2412-2429.
- [2] T.B. Gorji, A. Ranjbar, Thermal and exergy optimization of a nanofluid-based direct absorption solar collector, Renewable Energy, 106 (2017) 274-287.
- [3] M. Bouhaleb, H. Abbassi, Natural convection in an inclined rectangular enclosure filled by CuO-H₂O nanofluid, with sinusoidal temperature distribution, International Journal of Hydrogen Energy, 40(39) (2015) 13676-13684.
- [4] A. Boualit, N. Zeraibi, T. Chergui, M. Lebbi, L. Boutina, S. Laouar, Natural convection investigation in square cavity filled with nanofluid using dispersion model, International Journal of Hydrogen Energy, 42(13) (2017) 8611-8623.
- [5] M. Bovand, S. Rashidi, J. Esfahani, Enhancement of heat transfer by nanofluids and orientations of the equilateral triangular obstacle, Energy conversion and management, 97 (2015) 212-223.
- [6] S. Jayhooni, M. Rahimpour, Effect of different types of nanofluids on free convection heat transfer around spherical mini-reactor, Superlattices and Microstructures, 58 (2013) 205-217.
- [7] R. Jmai, B. Ben-Beya, T. Lili, Heat transfer and fluid flow of nanofluid-filled enclosure with two partially heated side walls and different nanoparticles, Superlattices and Microstructures, 53 (2013) 130-154.
- [8] D. Wen, Y. Ding, Experimental investigation into convective heat transfer of nanofluids at the entrance region under laminar flow conditions, International journal of heat and mass transfer, 47(24) (2004) 5181-5188.
- [9] Y. He, Y. Men, Y. Zhao, H. Lu, Y. Ding, Numerical investigation into the convective heat transfer of TiO₂ nanofluids flowing through a straight tube under the laminar flow conditions, Applied Thermal Engineering, 29(10) (2009) 1965-1972.
- [10] R.M. Moghari, A. Akbarinia, M. Shariat, F. Talebi, R. Laur, Two phase mixed convection Al₂O₃-water nanofluid flow in an annulus, International Journal of Multiphase Flow, 37(6) (2011) 585-595.
- [11] J. Buongiorno, Convective transport in nanofluids, (2006).
- [12] M. Corcione, M. Cianfrini, A. Quintino, Two-phase mixture modeling of natural convection of nanofluids with temperature-dependent properties, International Journal of Thermal Sciences, 71 (2013) 182-195.
- [13] M. Corcione, E. Habib, A. Quintino, A two-phase numerical study of buoyancy-driven convection of alumina-water nanofluids in

- differentially-heated horizontal annuli, International Journal of Heat and Mass Transfer, 65 (2013) 327-338.
- [14] H.A. Pakravan, M. Yaghoubi, Analysis of nanoparticles migration on natural convective heat transfer of nanofluids, International Journal of Thermal Sciences, 68 (2013) 79-93.
- [15] G.A. Sheikhzadeh, M. Dastmalchi, H. Khorasanizadeh, Effects of nanoparticles transport mechanisms on Al₂O₃-water nanofluid natural convection in a square enclosure, International Journal of Thermal Sciences, 66 (2013) 51-62.
- [16] F. Garoosi, S. Garoosi, K. Hooman, Numerical simulation of natural convection and mixed convection of the nanofluid in a square cavity using Buongiorno model, Powder technology, 268 (2014) 279-292.
- [17] M.A. Sheremet, T. Groşan, I. Pop, Free convection in shallow and slender porous cavities filled by a nanofluid using Buongiorno's model, Journal of heat transfer, 136(8) (2014).
- [18] M.A. Sheremet, I. Pop, M.M. Rahman, Three-dimensional natural convection in a porous enclosure filled with a nanofluid using Buongiorno's mathematical model, International Journal of Heat and Mass Transfer, 82 (2015) 396-405.
- [19] N. Hazeri-Mahmel, Y. Shekari, A. Tayebi, Numerical Study of Mixed Convection Heat Transfer in a Cavity Filled with NonNewtonian Nanofluids Utilizing Two-phase Mixture Model, Amirkabir Journal of Mechanical Engineering, 50(6) (2019) 1199-1212.
- [20] S.Y. Motlagh, H. Soltanipour, Natural convection of Al₂O₃-water nanofluid in an inclined cavity using Buongiorno's two-phase model, International Journal of Thermal Sciences, 111 (2017) 310-320.
- [21] S.Y. Motlagh, S. Taghizadeh, H. Soltanipour, Natural convection heat transfer in an inclined square enclosure filled with a porous medium saturated by nanofluid using Buongiorno's mathematical model, Advanced Powder Technology, 27(6) (2016) 2526-2540.
- [22] S.Y. Motlagh, E. Golab, A.N. Sadr, Two-phase modeling of the free convection of nanofluid inside the inclined porous semi-annulus enclosure, International Journal of Mechanical Sciences, 164 (2019) 105183.
- [23] G.A. Sheikhzadeh, M. Sepehrnia, M. Rezaie, M. Mollamahdi, Natural Convection of Turbulent Al₂O₃-Water Nanofluid with Variable Properties in a Cavity with a Heat Source and Heat Sink on Vertical Walls, Amirkabir Journal of Mechanical Engineering, 50(6) (2017) 1237-1250.
- [24] H. Sajjadi, M. Gorji, G. Kefayati, D. Ganji, Lattice Boltzmann simulation of turbulent natural convection in tall enclosures using Cu/water nanofluid, Numerical Heat Transfer, Part A: Applications, 62(6) (2012) 512-530.
- [25] F. Garoosi, G. Bagheri, F. Talebi, Numerical simulation of natural convection of nanofluids in a square cavity with several pairs of heaters and coolers (HACs) inside, International Journal of Heat and Mass Transfer, 67 (2013) 362-376.
- [26] V. Bianco, O. Manca, S. Nardini, Entropy generation analysis of turbulent convection flow of Al₂O₃-water nanofluid in a circular tube subjected to constant wall heat flux, Energy Conversion and Management, 77 (2014) 306-314.
- [27] S. Bahrehmand, A. Abbassi, Heat transfer and performance analysis of nanofluid flow in helically coiled tube heat exchangers, Chemical Engineering Research and Design, 109 (2016) 628-637.
- [28] F. Garoosi, F. Hoseinnejad, Numerical study of natural and mixed convection heat transfer between differentially heated cylinders in an adiabatic enclosure filled with nanofluid, Journal of Molecular Liquids, 215 (2016) 1-17.
- [29] M. Ghanbarpour, E.B. Haghigi, R. Khodabandeh, Thermal properties and rheological behavior of water based Al₂O₃ nanofluid as a heat transfer fluid, Experimental Thermal and Fluid Science, 53 (2014) 227-235.
- [30] P.A. Durbin, Near-wall turbulence closure modeling without "damping functions", Theoretical and computational fluid dynamics, 3(1) (1991) 1-13.
- [31] P. Durbin, Application of a near-wall turbulence model to boundary layers and heat transfer, International Journal of Heat and Fluid Flow, 14(4) (1993) 316-323.
- [32] P.A. Durbin, Separated flow computations with the k-epsilon-v-squared model, AIAA journal, 33(4) (1995) 659-664.
- [33] F.-S. Lien, G. Kalitzin, Computations of transonic flow with the v₂-f turbulence model, International Journal of Heat and Fluid Flow, 22(1) (2001) 53-61.
- [34] A. Sveningsson, L. Davidson, Assessment of realizability constraints in v₂-f turbulence models, International journal of heat and fluid flow, 25(5) (2004) 785-794.
- [35] S. Patankar, Numerical heat transfer and fluid flow, Taylor & Francis, 2018.
- [36] C. Ho, W. Liu, Y. Chang, C. Lin, Natural convection heat transfer of alumina-water nanofluid in vertical square enclosures: an experimental study, International Journal of Thermal Sciences, 49(8) (2010) 1345-1353.
- [37] R. Henkes, F. Van Der Vlugt, C. Hoogendoorn, Natural-convection flow in a square cavity calculated with low-Reynolds-number turbulence models, International Journal of Heat and Mass Transfer, 34(2) (1991) 377-388.
- [38] N.C. Markatos, K. Pericleous, Laminar and turbulent natural convection in an enclosed cavity, International journal of heat and mass transfer, 27(5) (1984) 755-772.
- [39] G. Barakos, E. Mitsoulis, D. Assimacopoulos, Natural convection flow in a square cavity revisited: laminar and turbulent models with wall functions, International journal for numerical methods in fluids, 18(7) (1994) 695-719.
- [40] M. Goodarzi, M.R. Safaei, K. Vafai, G. Ahmadi, M. Dahari, S.N. Kazi, N. Jomhari, Investigation of nanofluid mixed convection in a shallow cavity using a two-phase mixture model, International Journal of Thermal Sciences, 75 (2014) 204-220 1290-0729.

HOW TO CITE THIS ARTICLE

S. Yekani Motlagh. *Effect of Thermophoresis, Brownian and Turbulent Mass Fluxes in the Simulation of Two-Phase Turbulent Free Convection of Nanofluid Inside the Enclosure using v₂-f Model.* AUT J. Mech Eng., 4(4) (2020) 465-480.

DOI: [10.22060/ajme.2020.16761.5832](https://doi.org/10.22060/ajme.2020.16761.5832)



